Development of a compact 325 MHz proton interdigital *H*-mode drift tube linac with high shunt impedance

P. F. Ma (马鹏飞)[1,2,3] R. Tang (唐若),[1,2,3] Y. Yang (杨业),[4] S. X. Zheng (郑曙昕),[1,2,3,*]
W. B. Ye (叶文博),[1,2,3] M. W. Wang (王敏文),[4] W. L. Liu (刘卧龙),[4] B. C. Wang (王百川),[4]
Q. Z. Xing (邢庆子),[1,2,3] C. T. Du (杜畅通),[1,2,3] H. Y. Zhang (张化一),[1,2,3]
J. Li (李健),[5] X. L. Guan (关遐令),[1,2,3] X. W. Wang (王学武),[1,2,3]
Z. M. Wang (王忠明),[4,†] and M. T. Qiu (邱孟通)[4]

[1]*Key Laboratory of Particle and Radiation Imaging (Tsinghua University),*
Ministry of Education, Beijing 100084, China
[2]*Laboratory for Advanced Radiation Sources and Application, Tsinghua University,*
Beijing 100084, China
[3]*Department of Engineering Physics, Tsinghua University, Beijing 100084, China*
[4]*State Key Laboratory of Intense Pulsed Radiation Simulation and Effect, Xi'an 710024, China*
[5]*Nuctech Company Limited, Beijing 100084, China*

This paper describes the construction, rf measurement and tuning, rf conditioning, and beam commissioning of a compact 325 MHz interdigital *H*-mode (IH) drift tube linac (DTL) with modified KONUS (Kombinierte Null Grad Struktur, combined zero-degree structure) beam dynamics at Tsinghua University. This IH-DTL accelerates a proton beam from 3 MeV to 7 MeV in about 1 m. With a high rf frequency of 325 MHz, the cavity is designed to be compact while retaining a high average gradient of 4 MV/m. The efficient shunt impedance ZT^2 is 101 MΩ/m. The beam test results show good agreement with the beam dynamics design. The developed compact IH-DTL can be applied to the injectors of medical proton machines.

DOI: 10.1103/PhysRevAccelBeams.24.020101

I. INTRODUCTION

The interdigital *H*-mode drift tube linac (IH-DTL) was first proposed by J. P. Blewett in the 1950s [1]. It operates in the TE_{111} mode and provides efficient acceleration of light and heavy ions with β (the ratio of the velocity relative to the light speed) ranging from 0.01 to 0.25 [2–6]. With an effective shunt impedance ZT^2 over 100 MΩ/m and an average gradient over 3 MV/m, the IH-DTL has been widely used in heavy-ion accelerators [7–18]. Since 2007, the IH-DTL has been employed as the main component of injectors for medical synchrotrons [6,19,20]. It has great advantages for such injectors, which require a compact structure at low cost.

Two typical IH-DTLs have been operated successfully for particle therapy facilities. With KONUS (Kombinierte Null Grad Struktur, combined zero-degree structure)

*zhengsx@tsinghua.edu.cn
†wangzm02@qq.com

beam dynamics [21–23], the 216.8 MHz IH-DTL at HIT (the Heidelberg Ion Beam Therapy Center) can accelerate $^{12}C^{4+}$ ions or protons from 0.4 MeV/u to 7 MeV/u in 3.76 m [24–27]. ZT^2 is 125 MΩ/m. The 200 MHz IH-DTL at NIRS (the National Institute of Radiological Sciences) is designed with alternating-phase-focusing (APF) beam dynamics [14,28–31]. It can accelerate a $^{12}C^{4+}$ or proton beam from 0.6 MeV/u to 4 MeV/u in 3.44 m with a ZT^2 of 110 MΩ/m.

A higher accelerating field can be obtained by increasing the radio frequency (rf) for a fixed bravery factor b [32], i.e., the ratio of the maximum surface electric field E_s to the Kilpatrick limit E_k [33]: $b = E_s/E_k$. For example, E_k will increase by 20% when the frequency is increased from 200 MHz to 325 MHz. Moreover, the cavity can be more compact with higher rf frequency. To explore the feasibility of constructing an IH-DTL with a higher accelerating gradient while retaining a high ZT^2, a compact 325 MHz proton IH-DTL with modified KONUS beam dynamics has been designed at Tsinghua University, taking account of the multiturn injection requirements for a medical synchrotron [34,35]. The average gradient of 4 MV/m and ZT^2 of 115 MΩ/m can be achieved by optimizing the cell parameters with CST software [36], taking into account 25% additional losses. This IH-DTL is

expected to accelerate a proton beam from 3 MeV to 7 MeV in about 1 m. Thus, no internal focusing magnetic lens is needed be installed in the cavity. With this kind of KONUS—beam dynamics, a high operating frequency could be employed and hence a compact and cost-effective injector system could be designed.

Based on the above physical design of the 325 MHz IH-DTL, an IH-DTL cavity has been constructed, rf-measured, and tuned. Furthermore, the IH-DTL has been installed tentatively in the H$^-$ linac injector of the Xi'an 200 MeV Proton Application Facility (XiPAF) [37,38], and high-power conditioning and beam commissioning have been conducted.

This paper describes the construction, rf measurement and tuning, high-power conditioning, and beam commissioning of the 325 MHz IH-DTL. The remainder of the paper is organized as follows. Section II presents an overview of the physical design of the IH-DTL cavity. The mechanical design and construction of the cavity are described in Secs. III and IV, respectively. The rf measurement and tuning results are presented in Sec. V, and the rf conditioning of the cavity is illustrated in Sec. VI. In Sec. VII, the details of the beam commissioning of the cavity are described. Finally, conclusions are summarized in Sec. VIII.

II. PHYSICAL DESIGN OF THE IH-DTL

To meet the multiturn injection requirement for a medical synchrotron, a 325 MHz IH-DTL has been designed with modified KONUS beam dynamics. The details of the design process can be found in Refs. [34,39,40]. The IH-DTL is divided into three sections, for rebunching (−80°), 0° acceleration, and debunching (10°), respectively, which is a slightly different structure from the conventional KONUS design. The −80° rebunching section eliminates the buncher between the IH-DTL and the rf quadrupole (RFQ). The positive-phase design of the 10° debunching section helps focus the beam transversely and expand the beam phase. Thus, the distance between the IH-DTL and the downstream debuncher can be shortened. This short DTL tank has a length of 1.14 m with no focusing element inside, which increases ZT^2 and reduces the difficulty of construction. The main design parameters of this DTL are shown in Table I. The cavity power is calculated by CST software with a 25% margin.

Cell parameters, including the shapes of the drift tubes, stems, ridges, and g/L (where g is the gap length and L is the cell length), are optimized to maintain high shunt impedance Z. Slim drift tubes with a bore radius of 8 mm and a thickness of 3 mm are adopted to reach high Z. If other parameters are fixed, Z decreases with increasing β and increases with increasing g/L. To slow down the decrease in Z, g/L is designed to be increasing with the increase of β.

TABLE I. Main design parameters of the IH-DTL.

| Parameter	Value
Particle species	Proton
Input energy	3 MeV
Output energy	7 MeV
Input peak current	15 mA
Pulse width	10–40 μs
Repetition frequency	0.5 Hz
rf frequency	325 MHz
Unloaded quality factor	9000
Cavity power	189 kW (1.25*CST)
ZT^2	115 MΩ/m
Peak electric field	40 MV/m ($b = 2.3$)
Cell number	21
Tank length	1.14 m

III. MECHANICAL DESIGN

For the tank of the 325 MHz IH-DTL, a three-piece structure has been adopted, as shown in Fig. 1. The tank is divided into a central frame with ridges and two half-shells. To simplify the machining of the central frame, a racetrack-like cavity [Fig. 1(b)] is designed. The centers of the arcs of the two half-shells are on the center axis of the cavity. The diameters of these arcs vary from 196.9 mm at the low-energy end to 232.6 mm at the high-energy end to adjust the gap voltage distribution. The width of the central frame is constant and equals 100 mm. The total inner length is 982.9 mm. The outer dimension of the whole tank is 340 mm (width) ×300 mm (height) ×1143 mm (length) [41].

There are in total 12 ports on the two shells, positioned symmetrically: 8 for the tuners, 3 for the vacuum pumping, and 1 for the coaxial power coupler [Fig. 1(d)]. The inner diameter of each port is 68 mm. Thus, the positions of tuners, vacuum ports, and coupler can be exchanged with each other. This design increases the flexibility of tank tuning. No dynamic tuner is used on the IH-DTL, and the frequency of the cavity is controlled by adjusting the water temperature during rf conditioning and beam experiments. Water cooling channels are present only in the half-shells, since the duty cycle is low.

The main requirement with regard to machining tolerances is that the gap-voltage error should be limited to within ±3%. The length tolerance of the drift tubes (DTs) should be less than ±0.05 mm, while their central positioning tolerances should be within ±0.1 mm, ±0.05 mm, and ±0.1 mm in the x, y, and z directions, respectively, to constrain the errors in gap voltages induced by machining and assembly errors of the DTs [41]. The maximum surface electric field locates near the ends of the DTs between the gaps, and the requirement that the surface roughness (arithmetical mean height of the surface, S_a [42]) be ≤ 0.8 μm helps to reduce E_s and improves Z.
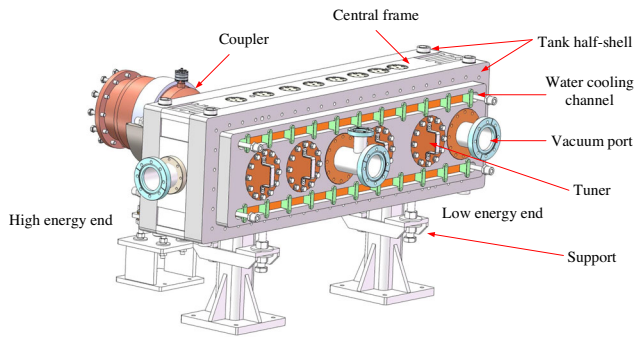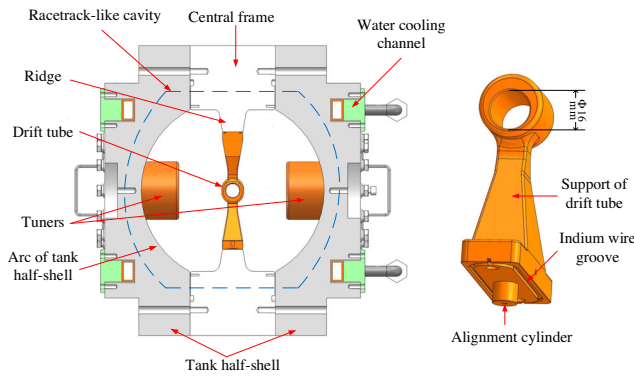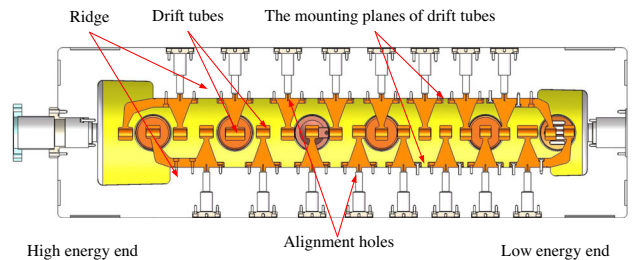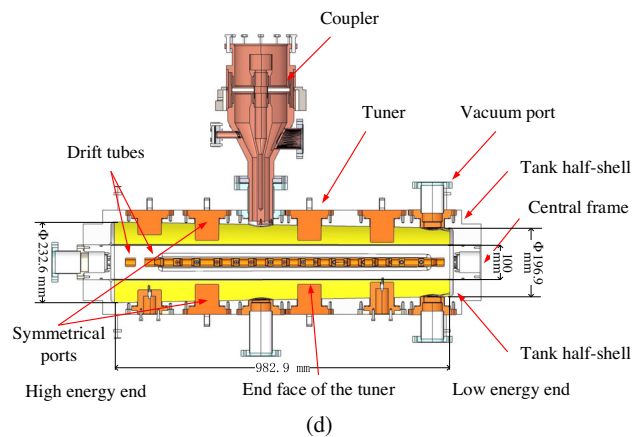
FIG. 1. (a) Mechanical design of the IH-DTL. (b) Main cross-sectional view of the IH-DTL and the drift tube. (c) Side cross-sectional view of the IH-DTL. (d) Top cross-sectional view of the IH-DTL.

IV. CONSTRUCTION

To facilitate machining, each of the DTs with its support was separately machined from copper blocks. The support is bolted to the up or down ridges. Indium wires are used to ensure rf contact between the ridges and supports of the DTs. A series of alignment holes on the ridges are used to match with the alignment cylinders [Fig. 1(b)] at the bottoms of the DTs, which is convenient for accurate assembly of the DTs. During assembly, the alignment cylinders can be trimmed to reduce alignment error.

The DTs were acid-pickled after machining to remove the copper oxide layer on their surfaces. After pickling, the surface roughness was measured with a 3D white light interferometer. S_a had deteriorated to 1.5 μm, which exceeds the tolerance of 0.8 μm, as shown in Fig. 2. To improve the surface roughness, metallographic sandpaper grinding and ultrasonic cleaning of the pickled DTs was conducted. After this surface treatment, S_a is improved to 0.13 μm.

The central frame and the shells were machined from mild carbon steel and their inner surfaces were nickel-plated and then copper-plated. The required thickness of the copper layer was 150 ± 20 μm. After the copper plating, the DTs were mounted and aligned on the frame, as shown in Fig. 3.

The alignment errors of the DT centers in the horizontal (x) and vertical (y) directions are each measured by a dial indicator. The longitudinal position errors of the DT centers
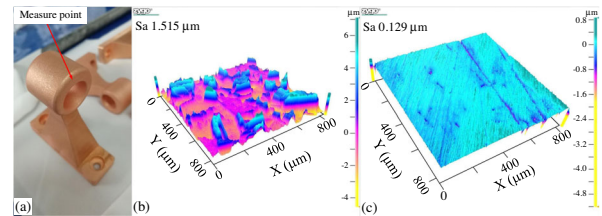

FIG. 2. Over-pickled DT and its surface roughness: (a) pickled DT; (b) surface roughness of pickled DT; (c) surface roughness of DT after surface treatment.
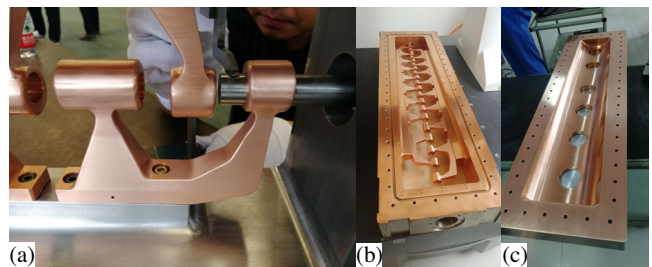

FIG. 3. Central frame with the aligned DTs and tank half-shell: (a) alignment of DTs; (b) central frame with DTs; (c) tank half-shell.
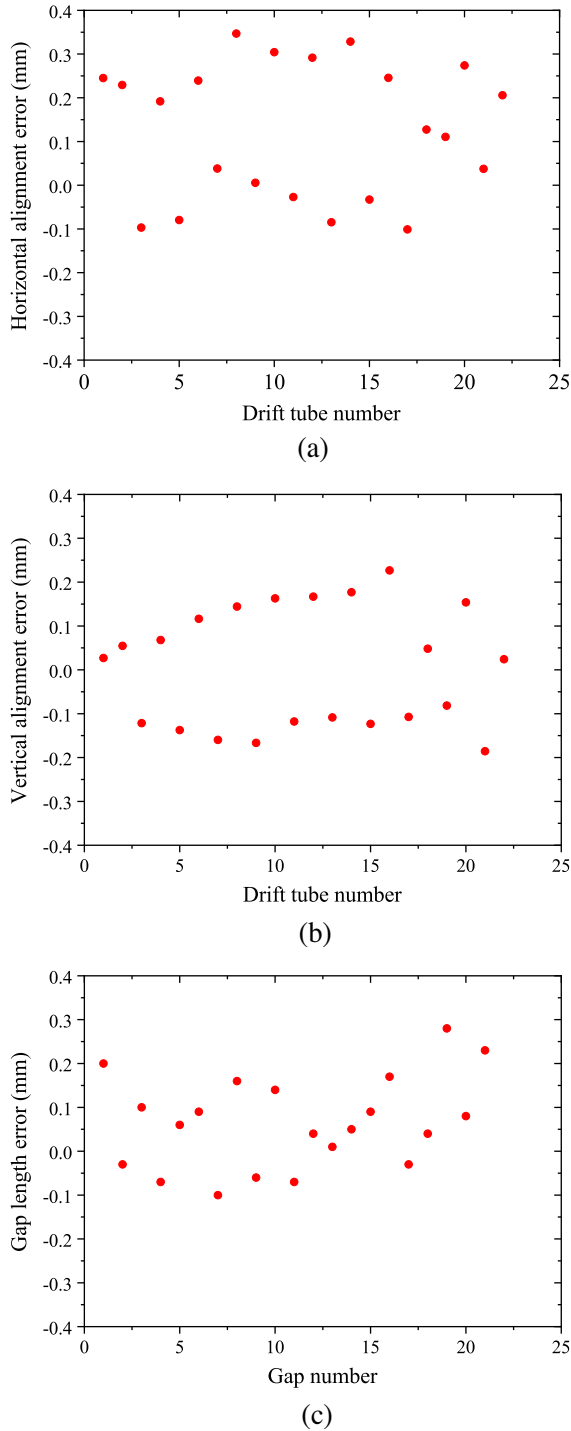
(a)

(b)

(c)

FIG. 4.   Position errors of the DT centers after alignment of the DTs: (a) horizontal error; (b) vertical error; (c) gap length error.

are measured indirectly by measuring the distance between the two DTs with gauge blocks and then checked by a coordinate measuring machine. For a DT with large alignment error, the alignment cylinder at its bottom [Fig. 1(b)] is trimmed to finely adjust its position. The final assembly error result for the DTs is shown in Fig. 4. The maximum range of all the errors from repeated measurement is
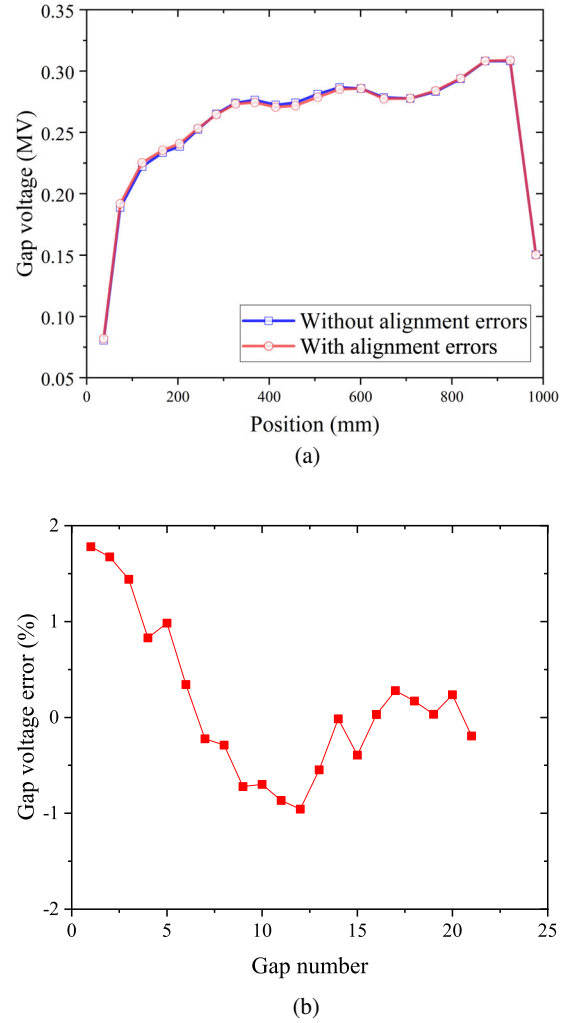

(a)

(b)

FIG. 5.   (a) Calculated gap voltage distribution along the beam axis. (b) Gap voltage error.

within ±0.03 mm. The measured assembly errors are the differences between the positions of all the DT centers and their fitting line. The fitting line is taken to be the beam center line of the IH-DTL cavity.

The maximum alignment errors of the DT centers are about ±0.3 mm in the x, y, and z directions. Although the alignment result exceeds the mechanical tolerance given in Sec. II, this does not mean that it is not acceptable, because there is some margin in the mechanical tolerance, which is derived by including the worst cases. To verify whether the measured errors are acceptable, they are incorporated into the cavity model, including tuners with the designed insertion depths, and the gap voltages are calculated by CST software. The calculated gap voltage and corresponding voltage error are shown in Fig. 5. The maximum gap voltage error is 1.8%, which is within the required tolerance of ±3% from the physical design. The beam dynamics simulation is then carried out, with the gap voltage error shown in Fig. 5(b) being taken into account. The relative
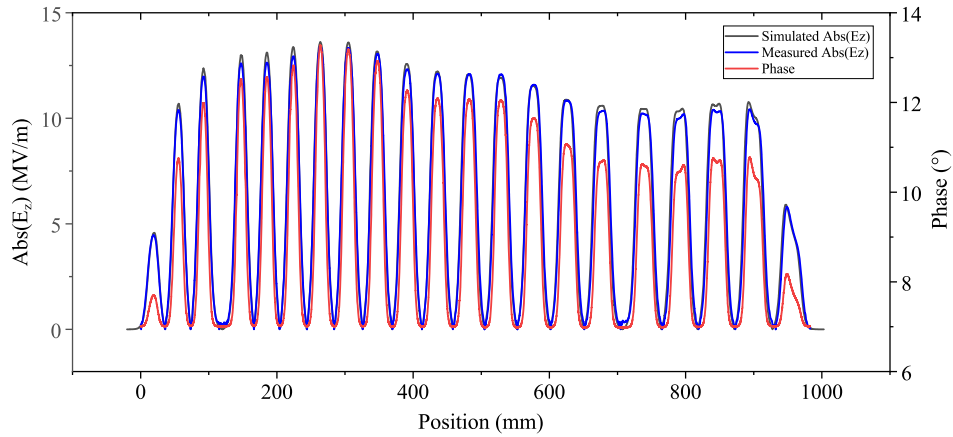
FIG. 6.   Phase and electric field distribution along the beam axis. The black curve is the electric field distribution simulated in the absence of DT errors, and the blue and red curves are the electric field distribution and S_{11} phase, respectively, measured by the bead perturbation method.

error in the transverse emittance compared with the design result is less than 3%, while the transmission stays the same and the energy difference is smaller than 0.15%. Therefore, the measured alignment result is acceptable.

V. rf MEASUREMENT AND TUNING

The tuning target of the IH-DTL cavity is to acquire a resonant frequency of 325 ± 0.01 MHz under operating conditions (25 °C, vacuum) and a relative error of the field distribution compared with the designed value within ±3%. The electric field distribution on the z axis of the cavity and the phase of the reflection S_{11} are obtained by the bead perturbation method [43] and are shown in Fig. 6, together with the electric field distribution simulated in the absence of DT errors.

The resonant frequency of the cavity operating mode is adjusted to around 325 MHz, and the frequencies of other modes are measured. Table II lists the measured and simulated frequencies of the modes inside the cavity. The first mode is the operating mode, which has the lowest resonant frequency. The frequency difference between the two lowest modes is 9.6 MHz. Unlike the Alvarez-type DTL, whose field sensitivity needs to be reduced by post-couplers [44], the IH-DTL has better stability of the internal field. Besides, the measured and simulated frequencies of different modes are in good agreement, which indicates that the electromagnetic field distribution inside the cavity is close to the designed value.

By fine adjustment of the insertion depths of four pairs of aluminum tuners (step size 0.1 mm), the cavity is tuned to 324.895 MHz (ambient temperature 25.8 °C, humidity 37.5%, cavity temperature 25.5 °C, and 101 kPa), and the field distribution is then close to the design. The relative error in the gap voltage is within ±3%.

The aluminum tuners are then successively replaced by copper ones. After each replacement, the remaining aluminum tuners are readjusted to satisfy the field distribution requirements. The final field distribution is shown in Fig. 7. The relative error in the gap voltage is smaller than ±3%, which is within the error tolerance and confirms that the measured alignment error is acceptable. The error bars come from random measurement error, which is within ±2%.

After tuning, the resonant frequency of the IH-DTL cavity reaches 324.920 MHz, and the unloaded quality factor is 7059. The ambient temperature is 19.5 °C, the humidity is 64%, the cavity temperature is 19.5 °C, and the pressure inside the cavity is 102.3 kPa. The corresponding resonant frequency under the operating conditions (25 °C, vacuum) is expected to be 324.997 MHz. The main reason of the difference between the physical design and the measured quality factor is that there are gaps of 0.5 mm width between the contact surfaces of the rf seal in the mechanical design to avoid virtual contact, and these are not taken into account in the physical model.

TABLE II.   Measured and simulated frequencies of modes inside the IH-DTL cavity.

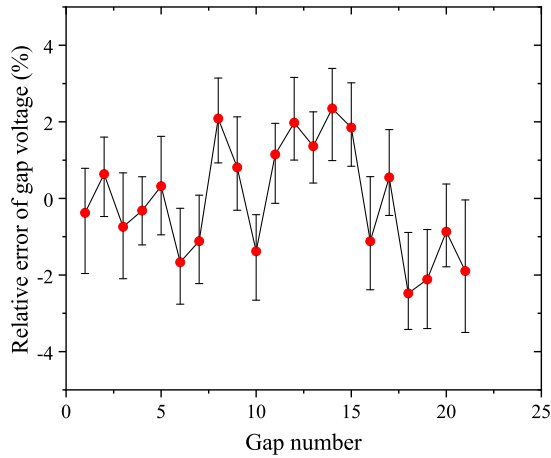| Mode	1	2	3	4	5	6
Measured frequency (MHz)	324.781	334.368	359.466	396.989	446.291	491.238
Simulated frequency (MHz)	324.935	334.911	359.614	397.219	446.301	491.012
Error (MHz)	−0.154	−0.543	−0.148	−0.23	−0.01	0.226

FIG. 7.   Relative error in gap voltage after tuning with copper tuners.

VI. rf CONDITIONING

Rf conditioning of the IH-DTL is performed to enhance the maximum achievable gradient by eliminating micro-protrusions and inclusions adsorbed on the inner surface of the cavity. A 4616 tetrode is used as the rf power source, with an output that is continuously adjustable from 20 kW to 500 kW [45].

The designed E_s of the IH-DTL cavity is 40 MV/m ($b = 2.3$), which is higher than that of common DTLs. The high-power rf conditioning of the cavity took about 50 h to reach the cavity power of 300 kW, with a repetition frequency of 1 Hz and a pulse width of 70 μs.

After rf conditioning, the time interval between adjacent rf breakdowns increases to more than 10 min. The static pressure of the cavity decreases from 8.5×10^{-5} Pa to 1.8×10^{-5} Pa, and the unloaded quality factor increases from 7059 to 7800, which is 87% of the designed value. The corresponding power loss of the cavity wall is 215 kW, ZT^2 is expected to be 101 MΩ/m.

VII. BEAM COMMISSIONING

After high-power rf conditioning, beam commissioning of the IH-DTL cavity is undertaken to verify its physical and mechanical design. The cavity is installed on the beamline of the H^- linac injector of XiPAF, downstream the RFQ accelerator. Beam commissioning is divided into two stages. The first stage is performed for the RFQ alone and the second for the joint of the RFQ and IH-DTL together.

A. Temporary beamline

The injector of XiPAF consists of an H^- electron cyclotron resonance (ECR) source, a low-energy beam transport system (LEBT), an RFQ, and an Alvarez-type DTL [38,46]. For beam commissioning of the IH-DTL, the Alvarez-type DTL is replaced by the IH-DTL. The temporary beamline is shown in Fig. 8. The XIPAF RFQ can provide an H^- beam with a current of 1.3 mA, an energy of 3 MeV, a repetition rate of 0.5 Hz, and a pulse width of 40 μs for beam commissioning. The temporary beamline downstream the RFQ consists of a beam matching section (BMS), the IH-DTL, and a test beamline.

The BMS between the RFQ and IH-DTL comprises three permanent magnet quadrupoles (PMQs) and a steering magnet. The test beamline downstream of the IH-DTL includes three quadrupole magnets and a 90° dipole magnet. Two AC current transformers (ACCTs) are used to measure the transmission of the BMS and the IH-DTL. One is located at the exit of the RFQ and the other at the exit of the IH-DTL. The horizontal and vertical phase spaces of the beam at the exit of IH-DTL are measured by an emittance meter. The beam energy at the exit of the IH-DTL is measured by the time-of-flight (TOF) method using two beam position monitors (BPMs) [47,48] and alternatively the dipole magnet. The beam energy spread is measured by the dipole magnet.

B. Beam commissioning for the separate RFQ

To verify the beam dynamics of the IH-DTL, its input and output beam distributions need to be measured. The input beam distribution of the BMS and IH-DTL, which is the output beam distribution of the RFQ, is used to simulate the beam dynamics to give the beam distribution at the exit of the IH-DTL. The measured and simulated beam distributions are compared to verify the physical design. Before the IH-DTL is mounted on the beamline, one emittance meter is installed at the exit of the RFQ, and beam commissioning of the RFQ is then carried out.

The XIPAF RFQ can accelerate an H^- beam from 50 keV to 3 MeV [49]. The length of the RFQ cavity is 3 m and the operating frequency is 325 MHz. Figure 9 shows the measured transverse phase spaces at the exit of the RFQ. The measured normalized RMS emittance at the exit of the RFQ is 0.43 πmm · mrad in the x–x' plane and 0.37 πmm · mrad in the y–y' plane. The current of the H^- beam at the exit of the RFQ is 1.3 mA. The transmission of the RFQ is 85%.

C. Design of the BMS

A special BMS including three PMQs is mounted between the RFQ and IH-DTL cavity to realize beam transverse matching. The PMQs are spares of the PMQs for the Alvarez DTL of XiPAF [50–52]. As the gradients of the existing PMQs are fixed, the distances between the PMQs are adjusted to match the beam to the IH-DTL. With a total length of 0.44 m, the mechanical design of the compact BMS is shown in Fig. 10. An ACCT is placed outside the ceramic. A steering magnet is added at the location of the second PMQ in the BMS to correct the eccentricity of the beam at the entrance of the IH-DTL, which can improve the transmission rate of the IH-DTL cavity.

The pipes of the BMS are connected by screws, and there is almost no adjustment allowance after installation.
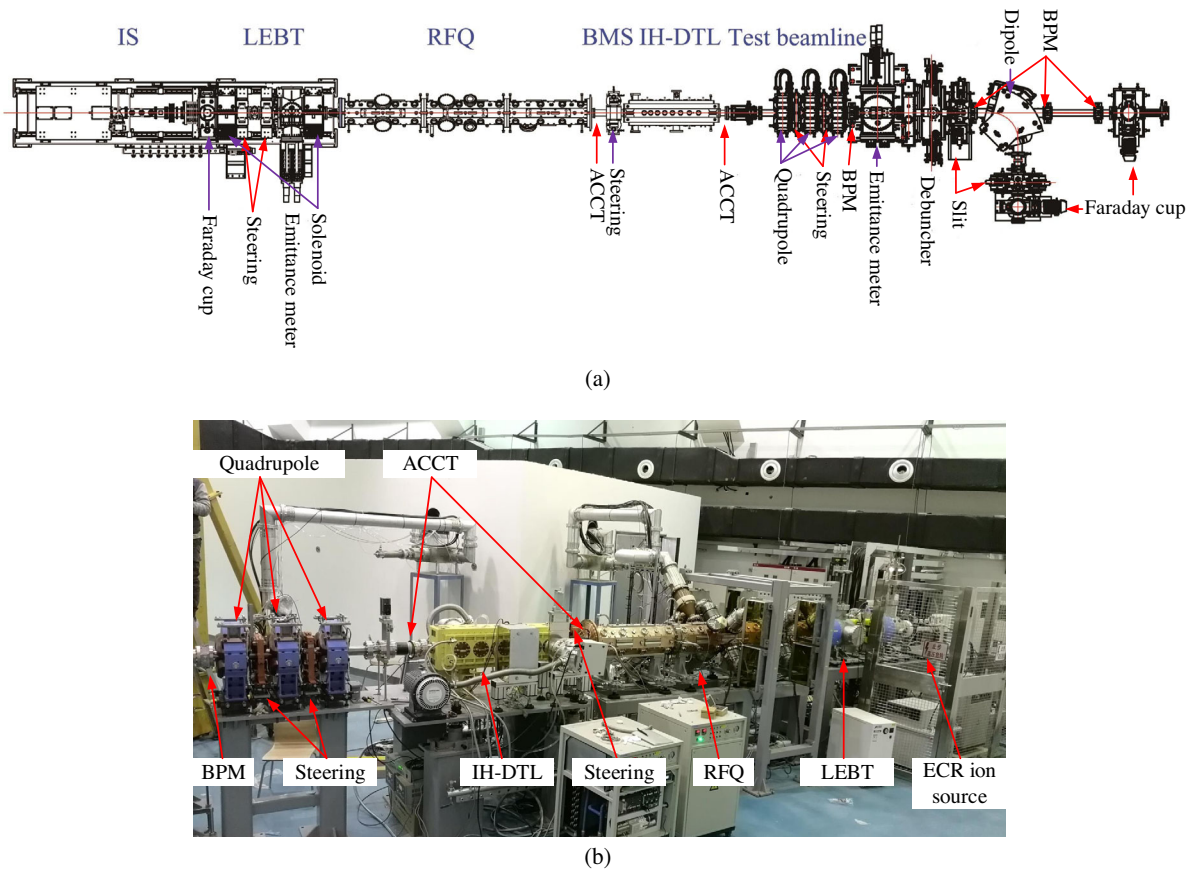
(a)

(b)

FIG. 8.   (a) XiPAF temporary beamline layout. (b) XiPAF temporary beamline from ion source to exit of IH-DTL.

The alignment errors of PMQs measured by the laser tracker are shown in Table III. The bore radii are 10 mm and the lengths are 40 mm for all the PMQs.

The beam distribution shown in Fig. 9 is taken as the input beam to simulate the beam dynamics inside the BMS and the IH-DTL cavity by the TRACEWIN code [53]. With the magnet alignment error in Table III taken into account, the beam transverse envelope in the BMS and IH-DTL cavity after steerer correction is shown in Fig. 11, and, according to the simulation result, the transmissions are 88% and 95% inside the BMS and IH-DTL, respectively.
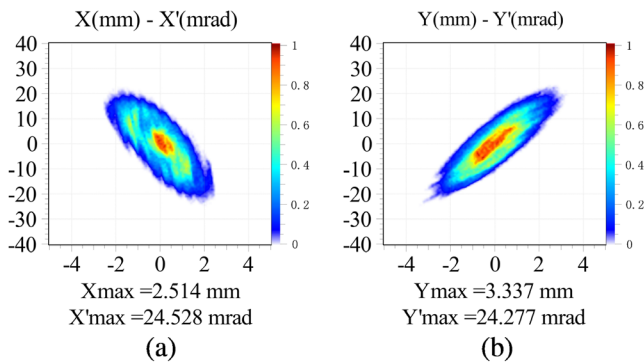
D. IH-DTL

The purpose of beam commissioning of the IH-DTL is to find the operating point of the cavity, including the rf power and the rf phase, and to measure the beam parameters at the exit of the IH-DTL to verify the physical design. The beam parameters include the transmission, energy, energy spread, and transverse phase space distribution. The test beamline of the IH-DTL is shown in Fig. 12.
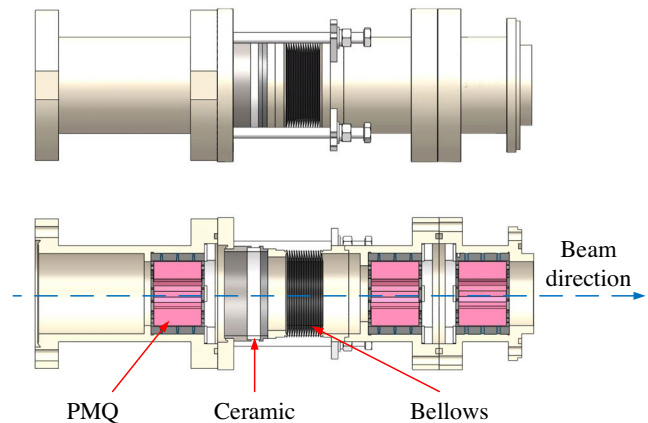

FIG. 9.   Measured phase spaces at the exit of the RFQ: (a) x–x' plane; (b) y–y' plane.

FIG. 10.   Mechanical design of the BMS.

TABLE III. Parameters and alignment errors of PMQs in the BMS.

	PMQ 1	PMQ 2	PMQ 3
Gradient (T/m)	82.4	−87.5	82.1
Horizontal position error (mm)	−0.21	−0.09	−0.02
Vertical position error (mm)	0.04	0.13	0.06
Longitudinal position error (mm)	0.31	−0.51	0.42

The variations of the simulated beam transmission and energy with rf power and phase are shown in Fig. 13. The normalized power level is the ratio of the rf power to the designed power. The rf phase ϕ_{input} is the input phase at the entrance of the IH-DTL of the beam dynamics design. The normalized power level and input rf phase at the operating point are 1 and −170°, respectively, which are selected according to the physical design. At the same power level, when $-270° < \phi_{\text{input}} < -190°$, although the transmission is higher than at the operating point, the output energy is below 6 MeV, which does not match the designed value of 7 MeV.

According to the rf conditioning results in Sec. VI, the incident power of the IH-DTL coupler at the operating point is estimated to be 220 kW, including the beam power. The beam load power of the IH-DTL cavity is 5.2 kW with a current of 1.3 mA, while the power loss of the cavity wall is 215 kW.

In the experiment, the transmission from the entrance of the BMS to the exit of the IH-DTL is measured while the

FIG. 12. Test beamline of the IH-DTL.

(a)

(b)

FIG. 13. (a) Transmission from the entrance of the BMS to the exit of the IH-DTL. (b) Variation of output energy with rf power and rf phase. The black point in each plot indicates the operating point of the IH-DTL.
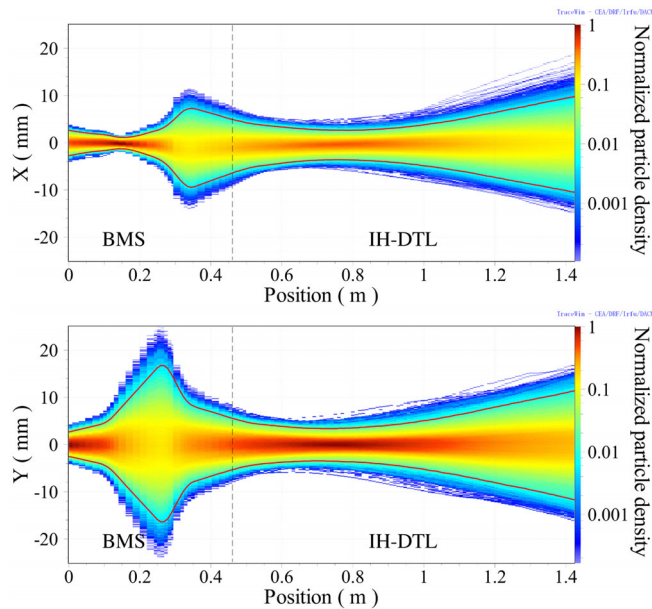

FIG. 11. Simulated beam envelope inside the BMS and the IH-DTL cavity after steerer correction, with the beam distribution at the exit of the RFQ as input and the alignment error of the BMS taken into account. The red curve represents the 99% beam envelope.
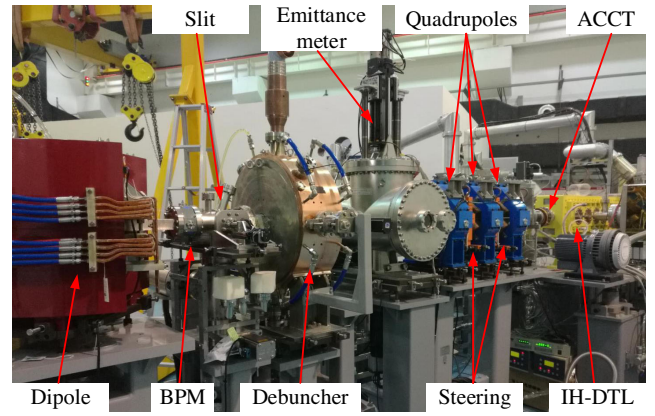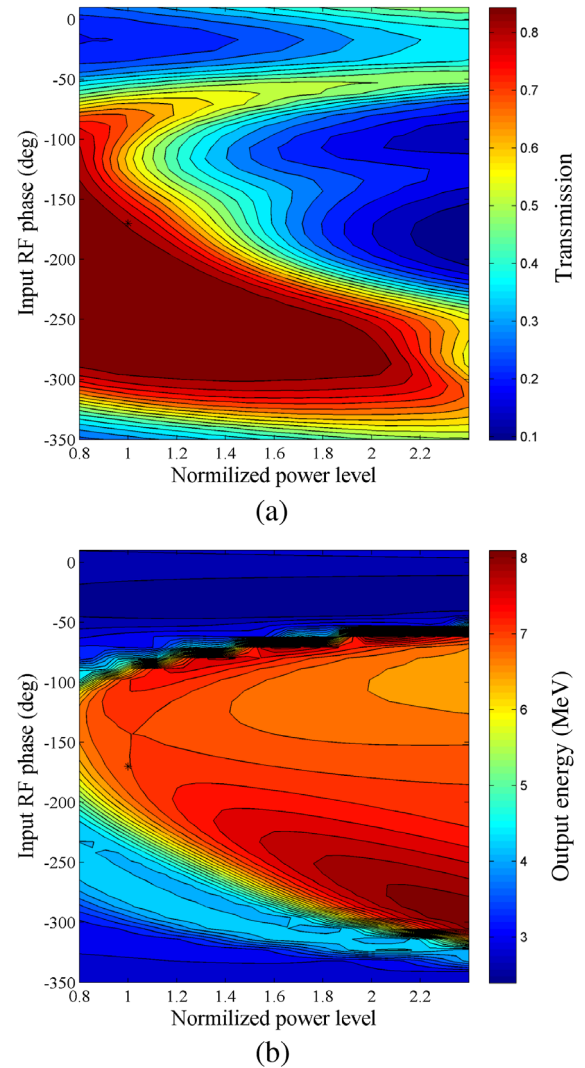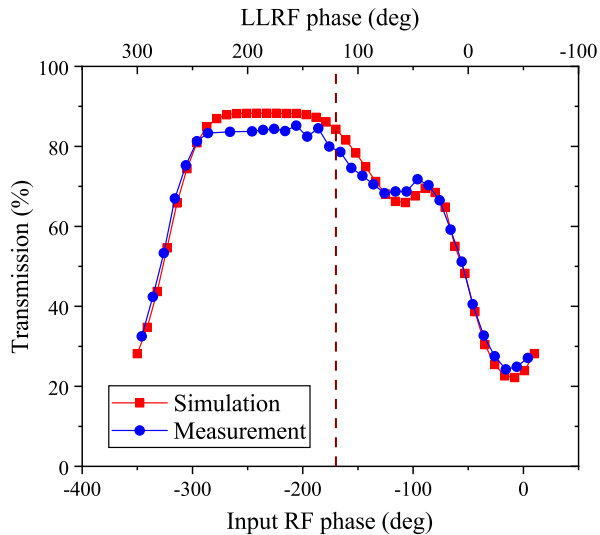
FIG. 14. Simulated transmission from the entrance of the BMS to the exit of the IH-DTL versus rf phase at 220 kW. The vertical red dashed line indicates the operating phase of the IH-DTL.

FIG. 15. Energy spread measurements with one 1.4 mm-width slit.

phase ϕ_{LLRF} of the low-level control system (LLCS) for the DTL power source is swept, with the results shown in Fig. 14. The incident power is fixed at 220 kW. On comparing these results with a simulation using the input rf phase ϕ_{input} as a variable, it can be seen that the transmission characteristics obtained by experiment and simulation are consistent, and a relation between the two phases can be obtained: $\phi_{\text{LLRF}} = -\phi_{\text{input}} - 50°$. Therefore, the operating point of the IH-DTL can be determined to be at $\phi_{\text{LLRF}} = 120°$ and an incident power of 220 kW. The overall measured transmission of the BMS and IH-DTL is 81%. Assuming the beam losses in the BMS to be 12% according to the simulation, the transmission of the IH-DTL is 92%, which is close to the simulated value of 95%.

Measurement of the energy of the output beam at the exit of the IH-DTL is based on the result for the first two BPMs. The speed of the pulse center can be calculated from $t = NT + T\Delta\phi/360$, where t is the flight time of the pulse center, N is the number of the integral cycles between the two BPMs, T is the rf cycle of 325 MHz, and $\Delta\phi$ is the phase difference between the two BPMs. At the operating point, the energy measured at the exit of the IH-DTL is 7.0 MeV, and the energy difference between measurement and simulation is within ± 0.1 MeV.

The energy spread is measured using the dipole magnet, with the operating point of the IH-DTL set. The relationship between magnet current and beam center energy is calibrated with the beam output from the RFQ during the separate RFQ commissioning. The corresponding current of the 2.97 MeV beam from the RFQ is 228.1 A. Therefore, the average energy of the beam at the IH-DTL exit can be obtained as 6.96 MeV with a magnet current of 349.5 A. This result is in good agreement with that from the TOF method. The current of the dipole magnet is scanned with
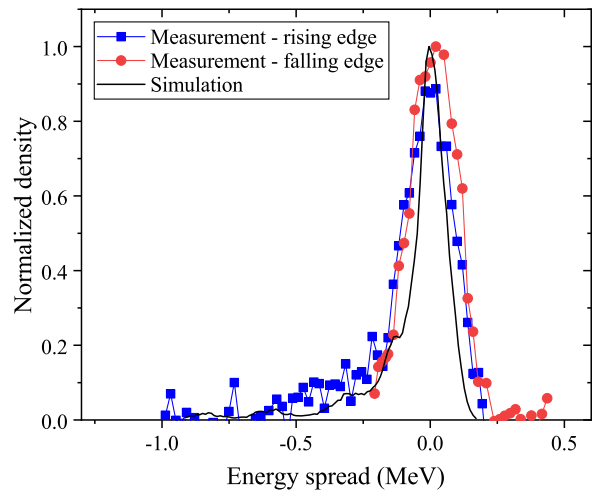
three slit widths. During each scan, the signal measured by a Faraday cup has a rising edge and a falling edge, which correspond to the energy distribution of the beam, with the rising and falling edges corresponding to the low- and high-energy parts, respectively. The results of measurements and simulation are shown in Fig. 15, where the average energy density has been normalized to 1. With one 1.4 mm-width slit, the measured energy spread is in good agreement with the simulation results. The energy spread in the simulation
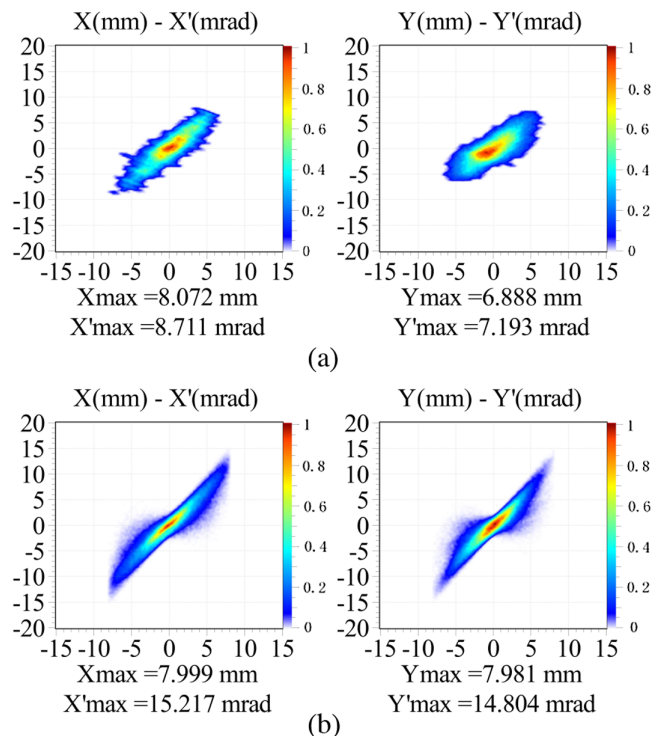

FIG. 16. (a) Measured and (b) simulated phase spaces at the exit of the IH-DTL: horizontal on the left; vertical on the right.

TABLE IV.   Beam Twiss parameters at the exit of the IH-DTL.

Parameters	α_x	β_x (mm/mrad)	Norm. RMS ε_x (π mm · mrad)	α_y	β_y (mm/mrad)	Norm. RMS ε_y (π mm · mrad)
Measurement	−1.79	1.75	0.58	−1.17	1.52	0.58
Simulation	−2.71	2.18	0.68	−2.22	1.87	0.58

at the exit of IH-DTL is from −0.4 MeV to 0.2 MeV, while the experimental result is from −0.6 MeV to 0.3 MeV.

The beam emittance downstream from the IH-DTL is measured with the quadrupole magnets powered off. During the measurements, the current of the vertical steering magnet in the BMS is set to 2 A to reduce the eccentricity of the beam in the *y* direction. Regardless of the eccentricity of the bunch, the measured beam phase space distribution is simulated back to the exit of IH-DTL, and the result is shown in Fig. 16. The Twiss parameters and emittance results at the exit of IH-DTL are shown in Table IV. The measurement results for the root mean square (RMS) phase ellipse of the beam are generally consistent with the simulation results. The measurement results show that the normalized RMS emittance of the IH-DTL is $0.58(x)/0.58(y)$ π mm · mrad, and the transverse emittance increases by 57%, which is in good agreement with the simulated emittance growth of 58% in Ref. [34].

VIII. CONCLUSIONS

A compact proton IH-DTL with a high ZT^2 of 115 MΩ/m has been designed for a typical medical synchrotron. With a high rf frequency of 325 MHz, the cavity is compact while retaining a high average gradient of 4 MV/m. The IH-DTL cavity has been successfully machined, assembled, tuned, and high-power conditioned. The difference between the measured and designed field distributions is within ±3% after tuning. After about 50 h of rf conditioning, the cavity has reached a cavity power level of 300 kW, an unloaded quality factor of 7800 (87% of the designed value), and a ZT^2 of 101 MΩ/m. Beam commissioning of the IH-DTL cavity has been successfully conducted on the beamline of the H$^-$ linac injector of XiPAF. At the exit of the IH-DTL, the measured average energy of the beam is 7.0 MeV, the energy spread range is −0.6 MeV to 0.3 MeV. The transverse normalized RMS emittance of the beam is $0.58(x)/0.58(y)$ π mm · mrad, with an input emittance of $0.43(x)/0.37(y)$ π mm · mrad. The beam transmission of the IH-DTL reaches 92%.

The experimental performance of the IH-DTL cavity verifies the design methodology including the beam dynamics and cavity design. The application of the IH-DTL with KONUS—beam dynamics is expanded to proton accelerators with beam tested. Furthermore, the developed compact IH-DTL can be employed as the main component of injectors for medical proton synchrotrons. The attractive advantages are cost-saving, easy-construction and quick-conditioning.

[1] J. Blewett, Linear accelerator injectors for proton-synchro-trons, in *CERN Symposium on High-Energy Accelerators and Pion Physics* (CERN, Geneva, Switzerland, 1956), pp. 159–166.

[2] P. N. Ostroumov, A. S. Plastun, N. Bultman, D. Morris, X. Rao, Q. Zhao, and S. Zhao, Efficient continuous wave accelerating structure for ion beams, Phys. Rev. Accel. Beams **23**, 042002 (2020).

[3] S. Benedetti, A. Grudiev, and A. Latina, High gradient linac for proton therapy, Phys. Rev. Accel. Beams **20**, 040101 (2017).

[4] M. Otani, T. Mibe, M. Yoshida, K. Hasegawa, Y. Kondo, N. Hayashizaki, Y. Iwashita, Y. Iwata, R. Kitamura, and N. Saito, Interdigital *H*-mode drift-tube linac design with alternative phase focusing for muon linac, Phys. Rev. Accel. Beams **19**, 040101 (2016).

[5] G. Clemente, U. Ratzinger, H. Podlech, L. Groening, R. Brodhage, and W. Barth, Development of room temperature crossbar-H-mode cavities for proton and ion acceleration in the low to medium beta range, Phys. Rev. Accel. Beams **14**, 110101 (2011).

[6] J. Qiao, X. C. Xie, D. M. Li, and Y. H. Pu, Physical design and multi-particle simulations of a compact IH-DTL with KONUS beam dynamics for proton therapy, Nucl. Sci. Tech. **31**, 64 (2020).

[7] G. Amendola *et al.*, A heavy ion linac for the CERN accelerator complex, in *Proc. EPAC92* (Berlin, Germany, 1992), pp. 536–538.

[8] "GSI website", (2020).

[9] W. Barth *et al.*, Commissioning of IH-RFQ and IH-DTL for the GSI high current linac, in *Proceedings of the 20th International Linac Conference, LINAC-2000, Monterey, CA, 2000* (SLAC, Menlo Park, CA, 2000), p. MOD11.

[10] J. Alessi *et al.*, Construction of the BNL EBIS preinjector, in *Proceedings of the 23rd Particle Accelerator*

Conference, Vancouver, Canada, 2009 (IEEE, Piscataway, NJ, 2009), p. MO6RFP025.

[11] M. Maier *et al.*, Commissioning of the linac for the Heidelberg heavy ion cancer therapy centre (HIT), in *Proceedings of the 22nd Particle Accelerator Conference, PAC-2007, Albuquerque, NM* (IEEE, New York, 2007), p. THPMN014.

[12] B. Schlitt *et al.*, Linac commissioning at the Italian hadrontherapy centre CNAO, in *Proceedings of the International Particle Accelerator Conference, Kyoto, Japan* (ICR, Kyoto, 2010), p. MOPEA003.

[13] H. Du *et al.*, RF design and cold model Mmasurement of an IH-DTL for HIMM injector, in *Proc. LINAC18, Beijing, China* (JACoW Publishing, Geneva, Switzerland, 2018), p. TUPO004.

[14] Y. Iwata *et al.*, Alternating-phase-focused IH-DTL for an injector of heavy-ion medical accelerators, Nucl. Instrum. Methods Phys. Res., Sect. A **569**, 685 (2006).

[15] A. M. Bazanov *et al.*, Light-ion linear accelerator for the NICA project, Phys. Part. Nucl. Lett. **17**, 481 (2020).

[16] K. D. Wang *et al.*, RF design of radio-frequency quadrupole accelerator for heavy ion medical machine, Nucl. Instrum. Methods Phys. Res., Sect. A **927**, 375 (2019).

[17] L. Lu, W. Ma, C. Li, T. He, L. Yang, L. Sun, X. Xu, W. Wang, and L. Shi, New developments of HIF injector, Matter Radiat. Extrem. **3**, 50 (2018).

[18] B. Mustapha, Z. Conway, M. Kelly, A. Plastun, and P. Ostroumov, Design of the multi-ion injector linac for the JLAB EIC (JLEIC), J. Phys. Conf. Ser. **1401**, 012008 (2020).

[19] B. Schlitt, Commissioning and operation of the injector linacs for HIT and CNAO, in *Proc. LINAC08, Victoria, BC, Canada* (JACoW Publishing, Geneva, Switzerland, 2008), p. WE205.

[20] X. Li, Y. H. Pu, F. Yang, X. C. Xie, Q. Gu, J. Qiao, and M. H. Zhao, RF design and study of a 325 MHz 7 MeV APF IH-DTL for an injector of a proton medical accelerator, Nucl. Sci. Tech. **30**, 153 (2019).

[21] U. Ratzinger, H. Hähnel, R. Tiede, J. Kaiser, and A. Almomani, Combined zero degree structure beam dynamics and applications, Phys. Rev. Accel. Beams **22**, 114801 (2019).

[22] U. Ratzinger, H-type linac structures, *CAS—CERN Accelerator School: Radio Frequency Engineering*, Tech. Rep. (CERN, Geneva, 2005).

[23] R. Tiede *et al.*, KONUS beam dynamics designs using H-mode cavities, in *Proc. HB08, Nashville, TN, USA* (JACoW Publishing, Geneva, Switzerland, 2008), p. WGB11.

[24] Y. R. Lu, U. Ratzinger, B. Schlitt, and R. Tiede, The general RF tuning for IH-DTL linear accelerators, Nucl. Instrum. Methods Phys. Res., Sect. A **582**, 336 (2007).

[25] Y. R. Lu *et al.*, The compact 20 MV IH-DTL for the Heidelberg therapy facility, in *Proc. LINAC04, Lübeck, Germany* (JACoW Publishing, Geneva, Switzerland, 2004), p. MOP11.

[26] Y.-R. Lu, Development of an IH-DTL injector for the Heidelberg cancer therapy project, Ph.D. thesis, Goethe University Frankfurt, 2005.

[27] G. Clemente *et al.*, Assembly and RF tuning of the IH-DTL for the HIT linac, Tech. Rep. (GSI, Darmstadt, Germany, 2006).

[28] I. M. Kapchinskiy and V. A. Teplyakov, A linear ion accelerator with spatially uniform hard focusing, Prib. Tekh. Eksp. **119**, 17 (1970).

[29] Y. Iwata, T. Fujimoto, N. Miyahara, T. Fujisawa, H. Ogawa, S. Yamada, T. Murakami, T. Mitsumoto, and H. Tsutsui, Model cavity of an alternating-phase-focused IH-DTL, Nucl. Instrum. Methods Phys. Res., Sect. A **566**, 256 (2006).

[30] Y. Iwata *et al.*, Performance of a compact injector for heavy-ion medical accelerators, Nucl. Instrum. Methods Phys. Res., Sect. A **572**, 1007 (2007).

[31] Y. Iwata *et al.*, Development of carbon-ion radiotherapy facilities at NIRS, IEEE Trans. Appl. Supercond. **28**, 4400807 (2018).

[32] T. P. Wangler, *RF Linear Accelerators*, 2nd ed. (Wiley, New York, 2008).

[33] W. D. Kilpatrick, Criterion for vacuum sparking designed to include both rf and dc, Rev. Sci. Instrum. **28**, 824 (1957).

[34] R. Tang, Q. Xing, S. Zheng, X. Guan, C. Tang, X. Wang, and J. Shi, IH-DTL design with modified KONUS beam dynamics for a synchrotron-based proton therapy system, Nucl. Instrum. Methods Phys. Res., Sect. A **920**, 50 (2019).

[35] P. F. Ma *et al.*, Physical design of a single-amplifier-driven proton linac injector for a synchrotron-based proton-therapy system in China, Nucl. Instrum. Methods Phys. Res., Sect. A **900**, 32 (2018).

[36] CST, CST Microwave Studio: Workflow & Solver Overview, Tech. Rep. (CST-GmbH, 2016).

[37] S. X. Zheng *et al.*, Overall design and progress of XiPAF project, in *Proc. SAP17, Jishou, China* (JACoW Publishing, Geneva, Switzerland, 2017), p. WECH2.

[38] Q. Z. Xing *et al.*, RF and primary beam dynamics design of a 325 MHz IH-DTL, in *Proc. IPAC16* (JACoW, Geneva, 2016), p. MOPMW014.

[39] R. Tang *et al.*, Beam dynamics of a 325 MHz IH-DTL with KONUS, in *Proc. SAP17, Jishou, China* (JACoW Publishing, Geneva, Switzerland, 2017), p. MOPH12.

[40] R. Tang *et al.*, RF and primary beam dynamics design of a 325 MHz IH-DTL, in *Proc. IPAC17* (JACoW, Geneva, 2017), p. TUPVA104.

[41] R. Tang *et al.*, Mechanical design and error analysis of a 325 MHz IH-DTL test cavity, in *Proc. IPAC18* (JACoW, Geneva, 2018), p. TUPAL075.

[42] ISO, ISO 25178-2:2012, Tech. Rep. (ISO, 2012).

[43] R. Tang *et al.*, Tuning and low power test of the 325 MHz IH-DTL at Tsinghua University, in *Proc. LINAC18, Beijing, China* (JACoW Publishing, Geneva, Switzerland, 2018), p. THPO035.

[44] Y. Lei *et al.*, Radio frequency measurement and tuning of a 13 MeV Alvarez-type drift tube linac for a compact pulsed hadron source, Rev. Sci. Instrum. **90**, 013302 (2019).

[45] Y. Lei *et al.*, High-power RF test of coaxial couplers for the injection linac of XiPAF, in *Proc. IPAC18* (JACoW, Geneva, 2018), p. THPAL110.

[46] Q. Z. Xing *et al.*, Design of the 7MeV linac injector for the 200MeV synchrotron of the Xi'an proton application facility, in *Proc. IPAC17* (JACoW, Geneva, 2017), p. TUPVA105.

[47] M. W. Wang, S. X. Zheng, Z. M. Wang, M. T. Qiu, X. L. Guan, W. H. Huang, and X. W. Wang, Beam momentum spread measurement using two beam position monitors at Xi'an Proton Application Facility, Rev. Sci. Instrum. **90,** 103305 (2019).

[48] M. Wang, Q. Xing, X. Guan, Z. Wang, M. Qiu, X. Wang, W. Huang, and S. Zheng, An online bunch length and momentum spread measurement method based on multiple BPMs, Nucl. Instrum. Methods Phys. Res., Sect. A **916,** 77 (2019).

[49] Q. Z. Xing *et al.*, Field tuning and rf measurements of the four-vane radio frequency quadrupole with ramped inter-vane voltage, Phys. Rev. Accel. Beams **22,** 020102 (2019).

[50] B. C. Wang *et al.*, The development of permanent magnet quadrupoles for XiPAF DTL, in *Proc. LINAC18, Beijing, China* (JACoW Publishing, Geneva, Switzerland, 2018), p. THPO033.

[51] B. C. Wang *et al.*, Vibrating wire measurements for the XiPAF permanent magnet quadrupoles, in *Proc. IPAC16* (JACoW, Geneva, 2016), p. TUPMB009.

[52] B. Wang, S. Zheng, Q. Xing, Z. Wang, C. Zhao, M. Qiu, and X. Wang, Measurements of the integrated gradient for Halbach-type permanent magnet quadrupoles, Nucl. Instrum. Methods Phys. Res., Sect. A **928,** 1 (2019).

[53] D. Uriot and N. Pichoff, TraceWin documentation, Tech. Rep. (CEA Saclay, 2020).